Contribution of *s-d* exchange interaction to magnetoresistance of ZnO-based heterostructures with a magnetic barrier

K. Masuko, A. Ashida, T. Yoshimura, and N. Fujimura
Department of Physics and Electronics, Graduate School of Engineering, Osaka Prefecture University, 1-1 Gakuen-cho, Naka-ku, Sakai, Osaka 599-8531, Japan
(Received 13 March 2009; revised manuscript received 22 July 2009; published 15 September 2009)

We report the origin of the positive magnetoresistance (MR) occurring in the ZnO conduction layer underneath of the $Zn_{0.88}Mn_{0.12}O$ magnetic barrier layer. First, *n*-type $Zn_{0.88}Mn_{0.12}O/ZnO$ modulation-doped heterostructures were fabricated on ZnO $(000\bar{1})$ single-crystal substrates using pulsed laser deposition. The MR characteristics of two heterostructures with different low-temperature electron mobility (μ), corresponding to the magnitude of interface broadening generated by intermixing or interdiffusion of Mn ions during deposition, were evaluated to investigate the mechanism of spin-related transport phenomena occurring at the heterointerface. The $Zn_{0.88}Mn_{0.12}O/ZnO$ heterostructure with high μ shows the Brillouin-function-like MR behavior, while that with low μ shows typical two-dimensional diluted magnetic semiconductor (2D DMS) MR behavior originating from the existence of Mn ions in the ZnO conduction layer. On the other hand, for a heterostructure with high μ, 2D DMS MR is eliminated from the MR due to suppress the interface broadening, and the spin splitting of the subband in ZnO channel is induced through the difference of the penetration probability of wave function of up-spin carriers and down-spin carriers into the $Zn_{0.88}Mn_{0.12}O$ barrier layer.

DOI: 10.1103/PhysRevB.80.125313 PACS number(s): 75.50.Pp, 73.43.Qt, 85.75.−d

I. INTRODUCTION

Diluted magnetic semiconductor (DMS) based heterostructures have demonstrated several spin related phenomena such as a spin-polarized transport and luminescence attributable to an *sp-d* exchange interaction.[1–4] Because such spin polarization can be tuned by application of an electric voltage or a magnetic field, novel spintronics devices are highly anticipated.

In fact, ZnO has great potential for use as a spintronics material because it has long spin-coherence time and length attributable to its large electron effective mass.[5] Regarding the DMS, $Zn_{1-x}Mn_xO$ with *p*-type conduction is theoretically predicted as a room-temperature ferromagnet,[6] suggesting that the critical issue of low Curie temperature in other DMS such as $Ga_{1-x}Mn_xAs$ would be settled. We have grown ZnO-based DMS/semiconductor heterostructures that contain magnetic impurities in the barrier layer on the sapphire (0001) and the ZnO $(000\bar{1})$ single-crystal substrates.[7–10] On the ZnO substrates, the $Zn_{1-x}Mn_xO/ZnO$ ($x \leq 0.14$) heterostructures with an atomically flat heterointerface and excellent crystallinity were fabricated successfully.[11] Regarding optical properties of the $Zn_{1-x}Mn_xO$ films, the band-edge transition in $Zn_{1-x}Mn_xO$ with $x=0.059$ epitaxial films was obtained by measuring the photoluminescence excitation spectra detected at the *d-d* transitions.[12] Also, the Mn concentration dependence of the band-edge transition showed a negative bowing profile in the Mn-composition region lower than $x=0.12$. Magnetization of the $Zn_{1-x}Mn_xO$ layers showed a typical paramagnetic behavior with the antiferromagnetic superexchange interaction between nearest-neighbor Mn ions through oxygen,[11] similarly to the magnetic properties of other Mn-doped II-VI semiconductors.[13] Up to $x=0.14$, a random distribution of Mn^{2+} ions substituted to the Zn^{2+} site was confirmed using magnetization[11] and extended X-ray absorption fine-structure measurements.[14] Regarding the *n*-type $Zn_{1-x}Mn_xO/ZnO$ modulation-doped heterostructures with $x=0.10$ and 0.12, the carrier confinement at the $Zn_{1-x}Mn_xO/ZnO$ heterointerface was confirmed.[7–10] The heterostructure showed the electron mobility (μ) greater than 10^3 $cm^2/V\,s$ at 10 K, which implies that it has longer spin coherence time and length than those of ZnO and ZnMnO bulk. Furthermore, we have reported that the positive magnetoresistance (MR) observed in the heterostructures can be fitted to the Brillouin function with $S=5/2$ and suggested the existence of *s-d* exchange interaction between *s* electrons in the ZnO channel and Mn *d* spins in the $Zn_{0.88}Mn_{0.12}O$ barrier.[8] This was the first observation of the MR behavior for heterostructures with the magnetic barrier. However, the origin of such a Brillouin-function-like positive MR has not been elucidated. Furthermore, if *p*-type conduction in the heterostructures is obtained, the spin-polarized current above RT is expected to be generated by ferromagnetic exchange interaction between the *p* hole in the ZnO channel and *d* spin in the ZnMnO barrier. Therefore, we have searched for spin-related phenomena between ZnO channel and ZnMnO barrier.

As described in this paper, we discuss the contribution of *d* spin in the $Zn_{0.88}Mn_{0.12}O$ magnetic barrier to the spin-dependent transport using an *n*-type $Zn_{0.88}Mn_{0.12}O/ZnO$ modulation-doped heterostructure. To investigate the spin-dependent transport which occurred at the $Zn_{0.88}Mn_{0.12}O/ZnO$ heterointerface, the correlation between the low-temperature μ and the spin-dependent transport is also discussed because the low-temperature μ is very sensitive to the magnitude of interface broadening generated by intermixing or interdiffusion of Mn ions. Comparison of the MR behaviors of two samples with different μ would clarify the origin of MR.

II. EXPERIMENTAL DETAILS

A. Samples

The $Zn_{0.88}Mn_{0.12}O/ZnO$ modulation-doped heterostructures were fabricated on the ZnO $(000\bar{1})$ single-crystal sub-

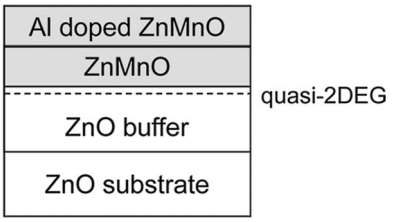

FIG. 1. Schematic of the $Zn_{0.88}Mn_{0.12}O$ modulation-doped heterostructure grown on the ZnO $(000\bar{1})$ single-crystal substrate.

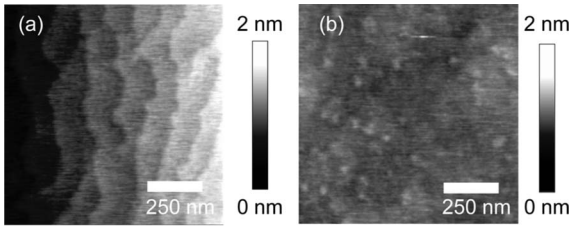

FIG. 2. AFM images of the surfaces for samples (a) A and (b) B.

strates (Tokyo Denpa Co., Ltd.) using pulsed laser deposition (PLD).[8–10] For this study, we, respectively, selected two samples having high μ and low μ; they were labeled as A and B. Figure 1 portrays the sample structure of $Zn_{0.88}Mn_{0.12}O/ZnO$. The deposition conditions are presented in Table I. The ZnO, $Zn_{0.90}Mn_{0.10}O$, and Al-doped $Zn_{0.90}Mn_{0.10}O$ ceramic targets were used for each deposition. The Al concentrations of samples A and B were, respectively, 0.001 and 0.005 at. %. Prior to deposition, the ZnO substrates were annealed at 950 °C for 10 h in air to form a surface with a step-and-terrace structure. Nondoped ZnO buffer layers with the thickness of d_b were deposited on the ZnO substrate at the growth temperature (T_{g_1}) of 670 °C. Atomic force microscopic (AFM) observation of the ZnO buffer layer showed a step-and-terrace structure with the step height of 0.26 nm, corresponding to a half unit length of a ZnO crystal. Subsequently, a $Zn_{0.88}Mn_{0.12}O$ spacer layer with the thickness of d_s and an Al-doped $Zn_{0.88}Mn_{0.12}O$ doping layer with the thickness of d_d were deposited, respectively, at the growth temperature (T_{g_2}) of 640 and 670 °C for samples A and B. The surface morphology and crystallographic characteristics of the $Zn_{0.88}Mn_{0.12}O$ layer were evaluated using *in situ* reflection high-energy electron diffraction analysis, *ex situ* AFM (NanoScope E; Toyo Technica Inc.) and high-resolution X-ray diffraction analysis (X'pert-MRD; Philips Co.). The sheet resistance (ρ_s), the sheet carrier concentration (n_s) and μ were evaluated at temperatures of 10–300 K using Hall effect measurement in a van der Pauw configuration. A magnetic field of 0.5 T was applied perpendicular to the sample surface. The values of ρ_s, n_s, and μ measured at 10 K are listed in Table I together with the deposition conditions. Also, we characterized the magnetic field dependence of the Hall effect for samples A and B under applied magnetic fields below 5 T. At 10 K, the Hall voltage was linearly proportional to magnetic field, indicating that they show no anomalous Hall effect.

B. MR measurement

For this study, MR measurements were conducted at temperatures of 1.85–100 K. The sheet resistivity of the ZnO substrate at room temperature shows 100 Ω cm, corresponding to the sheet resistance ρ_s=2000 Ω/□. However, below around 100 K, the sheet resistance of the substrate markedly increases with decreasing temperature, and reaches more than 10 000 Ω/□ at 50 K. Also, we reported that Mn-doped ZnO films have much higher resistivity than nondoped ZnO.[15] Therefore, temperature ranges of less than 100 K for sample A and 50 K for sample B were used to eliminate the effects of parallel conduction in the ZnO substrate and $Zn_{0.88}Mn_{0.12}O$ barrier for analysis of these MR behaviors. Furthermore, the MR behavior of $Zn_{0.88}Mn_{0.12}O/ZnO$ heterostructure could be explained using the theoretical MR in low-dimensional system, as described in Sec. III. Also, we have characterized the MR behaviors for other $Zn_{0.88}Mn_{0.12}O/ZnO$ heterostructrues with different $Zn_{0.88}Mn_{0.12}O$ layer thickness, and found that the MR behavior in low-dimensional system did not change, supporting no influence of parallel conduction in the $Zn_{0.88}Mn_{0.12}O$ barrier. A magnetic field was applied parallel to the surface and the current to eliminate the contribution of the Lorentz force and weak localization effect induced in the MR.[8] We measured the MR in four-terminal configurations to eliminate the contribution of contact resistance at the interface between indium electrode and Al-doped ZnMnO layer. The MR was obtained using a standard ac lock-in technique with current (I) of 0.01–1 μA.

III. EXPERIMENTAL RESULTS AND DISCUSSION

A. Interface broadening at the $Zn_{0.88}Mn_{0.12}O/ZnO$ heterointerface

The electron mobility μ for samples A and B measured at 10 K were 1020 and 240 cm^2/V s, respectively, as presented in Table I. The surface roughness and the crystallinity of samples A and B were investigated to elucidate the origin for the difference of μ. Figures 2(a) and 2(b), respectively, portray AFM images of surfaces for samples A and B. For sample A with high μ, the surface of Al-doped $Zn_{0.88}Mn_{0.12}O$

TABLE I. Growth parameters and values of ρ_s, n_s, and μ measured at 10 K.

	ZnO	Buffer	ZnMnO, ZnMnO:Al			Hall Measurement at 10 K		
Sample	T_{g_1} (°C)	d_b (nm)	T_{g_2} (°C)	d_s (nm)	d_d (nm)	ρ_s (Ω/□)	n_s ($\times 10^{12}$ cm^{-2})	μ (cm^2/V s)
A	670	180	670	64	16	1820	3.35	1020
B	670	440	640	10	30	5290	4.92	240

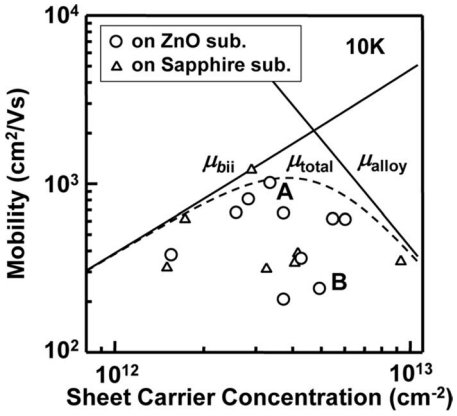

FIG. 3. The electron mobility μ as a function of sheet carrier concentration n_s in $Zn_{0.88}Mn_{0.12}O/ZnO$ heterostructures grown on the ZnO substrates (open circles) and $Zn_{0.90}Mn_{0.10}O/ZnO$ heterostructures grown on the sapphire substrates (open triangles). The contributions of different scattering mechanisms to the electron mobility are shown by solid lines. The broken curve represents the total electron mobility.

layer shows a step-and-terrace structure, similarly to that of the ZnO substrate, while the surface for the no step-and-terrace structure is recognized in sample B. However, the root mean square values of surface roughness for both samples were much smaller than 0.1 nm. In the X-ray diffraction 2θ-ω profiles around 0004 diffraction, clear interference fringes were observed not only for sample A, but also for sample B, indicating that they both have an atomically flat surface and interface. The full width at half maximum of the X-ray ω rocking curve measured at 0004 ZnMnO for samples A were 0.05°, which is identical to that of sample B. These results suggest that the $Zn_{0.88}Mn_{0.12}O$ layers of both samples have small surface roughness and excellent crystallinity, although the samples have quite different μ. In addition to these samples, low-temperature μ was evaluated for the other heterostructures with n_s ranging from 1.6×10^{12} to $9.3\times10^{12}(cm^{-2})$. The dominant scattering mechanisms at 10 K were discussed using the plot of μ vs n_s. Figure 3 shows the low-temperature μ as a function of n_s for the $Zn_{0.88}Mn_{0.12}O/ZnO$ modulation-doped heterostructures grown on the ZnO $(000\bar{1})$ single-crystal substrates and $Zn_{0.90}Mn_{0.10}O/ZnO$ modulation-doped heterostructures grown on *c*-plane sapphire substrates. The heterostructures show n_s ranging from 1.6×10^{12} to $9.3\times10^{12}(cm^{-2})$ and μ ranging from 240 to 1210$(cm^2/V\ s)$. In the heterostructures, low-temperature μ is expected to be limited by impurity scattering μ_{ii}, alloy disorder scattering μ_{ad}, and interface roughness scattering μ_{ir}.[16] The dominant scattering mechanisms for the $Zn_{0.88}Mn_{0.12}O/ZnO$ heterostructures are discussed as follows. Compared with the crystallinity and μ for the heterostructures grown on sapphire substrates, the interface roughness and the crystallinity for the heterostructures grown on ZnO substrates were drastically improved, whereas the enhancement of μ was not observed. Therefore, the electron mobility in a higher n_s region than around $4\times10^{12}(cm^{-2})$ is assumed to be limited by μ_{ad}. On the other hand, in lower n_s region, background ionized-impurity scattering μ_{bii} or remote ionized-impurity scattering μ_{rii} will become dominant. In our samples, the increase in μ in the thickness of spacer layer[17] was not obtained, suggesting that the background-ionized impurities will allow the suppression of μ in low n_s region. The background ionized impurities in the $Zn_{0.88}Mn_{0.12}O/ZnO$ heterostructures would be originated from the ceramic targets for laser ablation. The inverse of the total electron mobility $1/\mu_{total}$ can be calculated from the sum of the electron mobility for the individual processes

$$\frac{1}{\mu_{total}} = \frac{1}{\mu_{ad}} + \frac{1}{\mu_{bii}}. \quad (1)$$

To calculate μ_{ad} and μ_{bii}, we followed the equations in Refs. 18 and 19, respectively. In our calculation of μ_{ad}, the difference of conduction-band minima of MnO and ZnO, $\langle V\rangle$, and unit-cell volume, W, are 2.0 eV[20] and 36.1 Å,[3] respectively. μ_{ad} and μ_{bii} were calculated with the conduction-band offset (ΔE_c) of 0.4 eV and background ionized-impurity concentration (N_D) of 10^{18} cm^{-3}. The result is shown in Fig. 3. Here, μ is considered to be limited by μ_{bii} in the n_s region less than 4.8×10^{12} (cm^{-2}) and μ_{ad} in the n_s region greater than 4.8×10^{12} (cm^{-2}). For some samples including sample A, considering μ_{ad} and μ_{bii}, it is found that the calculated μ_{total} are in agreement with the experimental μ, suggesting that they have similar structure of interface broadening. However, other samples including sample B show much lower μ than calculated one. This discrepancy is probably attributable to the existence of the interface broadening generated by intermixing or interdiffusion of Mn ions during deposition. So far, in a $La_{0.7}Sr_{0.3}MnO_3/SrTiO_3$ multilayer fabricated using PLD system, the atomic-scale chemical imaging of composition and bonding has showed chemical intermixing at the $La_{0.7}Sr_{0.3}MnO_3/SrTiO_3$ heterointerface.[21] Such intermixing or interdiffusion at the heterointerface is assumed to be in our heterostructures. When the Mn ions are doped ZnO channel, the alloy scattering[22,23] and impurity scattering should be enhanced. Therefore, μ is assumed to be very sensitive to the change in the interface structure, because two-dimensional (2D) electrons are conducting in a few monolayers of ZnO surface.

B. Magnetoresistance

The MR behavior for the $Zn_{0.88}Mn_{0.12}O/ZnO$ heterostructures with different μ were investigated to discuss the contribution of *s-d* exchange interaction to the MR. Figures 4(a) and 4(b), respectively, show the temperature dependence of MR behaviors for samples A and B. For both samples, the positive MR is dominantly observed. The magnitude of a positive MR decreases concomitantly with increasing sample temperature. At temperatures greater than 50 K, the observed MR becomes negligibly small. The behavior of a positive MR for sample A with high μ can be well fitted to the Brillouin function with $S=5/2$, shown as a broken line, whereas that for sample B with low μ is in disagreement with the Brillouin function. Furthermore, the slope of a positive MR for sample B is larger than that of sample A. Based on these results, it is anticipated that the *s-d* exchange interaction is responsible for the positive MR and that the suppression of

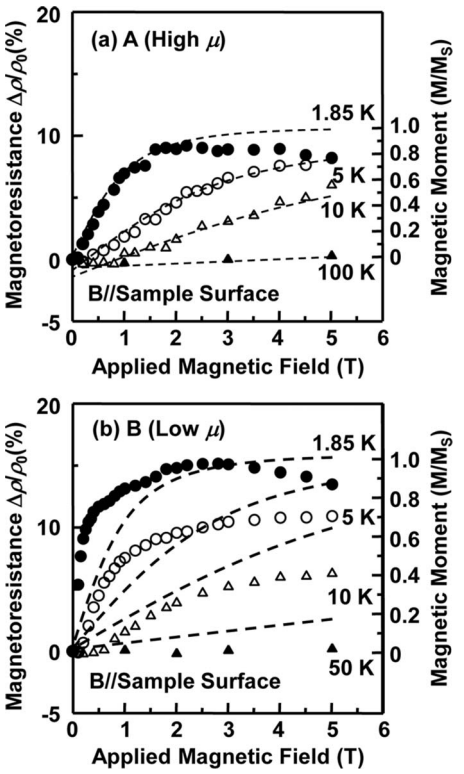

FIG. 4. Comparison of MR for samples (a) A and (b) B measured at 1.85 K (closed circles), 5 K (open circles), 10 K (open triangles), and 50 and 100 K (closed triangles). The broken lines represent the Brillouin function using $S=5/2$.

interface broadening should be quite important for obtaining the *s-d* exchange interaction at the $Zn_{0.88}Mn_{0.12}O$ barrier/ZnO channel layer interface.

C. Positive magnetoresistance of Mn-doped II-VI DMS

For Mn-doped II-VI DMS including ZnMnO thin films, the MR consists of the negative component and the positive component.[24] Negative MR has been understood through field-induced suppression of the magnetic field on weak localization[25,26] or strong localization.[27] On the other hand, positive MR has been modeled by accounting for the quantum correction of spin splitting on the disorder-modified electron-electron interaction. The interaction arises from coupling of the *s* conduction electrons to the spins of 3*d* localized magnetic moments of Mn^{2+} ions and produces a giant energy gap, so-called spin-splitting energy, between the up-spin conduction band and the down-spin conduction band. This spin-disorder-modified scattering, corresponding to positive MR, is introduced by the electron-electron interaction between the up-spin electron and the down-spin electron.[20]

D. Correlation between the spin splitting induced in $Zn_{0.88}Mn_{0.12}O$ and ZnO layers

To discuss the mechanism of the MR occurring in ZnO channel layer underneath the $Zn_{0.88}Mn_{0.12}O$ barrier layer, correlation between the spin splitting of conduction band of

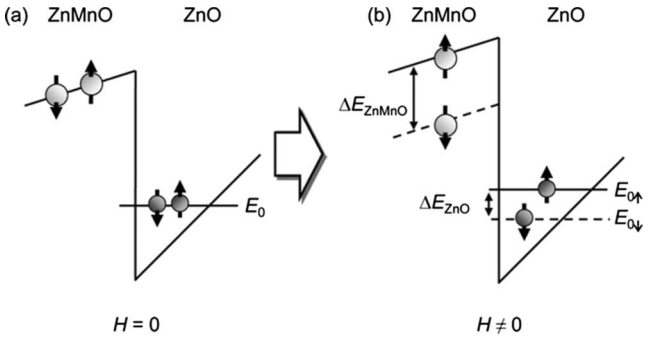

FIG. 5. Illustrative diagrams of band alignment of the conduction band for the $Zn_{0.88}Mn_{0.12}O/ZnO$ heterostructure (a) with and (b) without applying the magnetic field. E_0 represents the energy level of subband in the ZnO channel layer.

$Zn_{0.88}Mn_{0.12}O$ barrier and the subband in ZnO channel layer is specifically examined. The schematic of the band structure of $Zn_{0.88}Mn_{0.12}O/ZnO$ heterostructure (a) without and (b) with external magnetic field (H) are portrayed in Fig. 5. By applying a magnetic field, a giant spin splitting in $Zn_{0.88}Mn_{0.12}O$ barrier (ΔE_{ZnMnO}) is induced via *s-d* exchange interaction. The equation to express ΔE_{ZnMnO} is shown as Eq. (2)

$$\Delta E_{ZnMnO}(H) = g\mu_B H + x_{eff}\alpha N_0 S B_s(H), \tag{2}$$

where g is the Lande g factor, μ_B is the Bohr magneton, H is the applied magnetic field, x_{eff} is the effective mole fraction of the magnetic ions, αN_0 is the *s-d* exchange energy, and B_s is the Brillouin function for spin $S=5/2$. As g, x_{eff}, and αN_0, 2.0, 0.042,[11] and 0.19 eV[20] were used, respectively, in our calculations. The first and the second terms correspond to the Zeeman and the *s-d*, exchange interaction contributions, respectively. The solid line in Fig. 6 marks the calculated magnetic field dependence of ΔE_{ZnMnO} at 2 K. The ΔE_{ZnMnO} increases concomitantly with increasing H, and asymptotically reaches approximately 20 meV greater than 3 T. The Zeeman term $g\mu_B H$, which is presented as a broken line, is calculated as 0.58 meV at 5 T, suggesting that the Zeeman term is negligible for calculation of ΔE_{ZnMnO}. Therefore, ΔE_{ZnMnO} is given approximately as

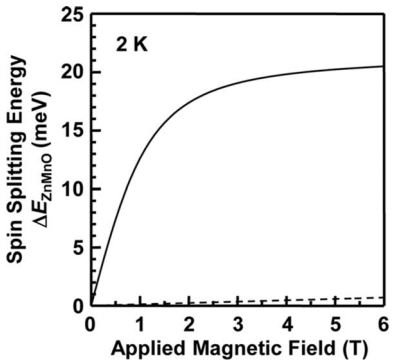

FIG. 6. Spin-splitting energy (solid line) of $Zn_{0.88}Mn_{0.12}O$ barrier layer at 2 K. The broken line shows the Zeeman contribution.

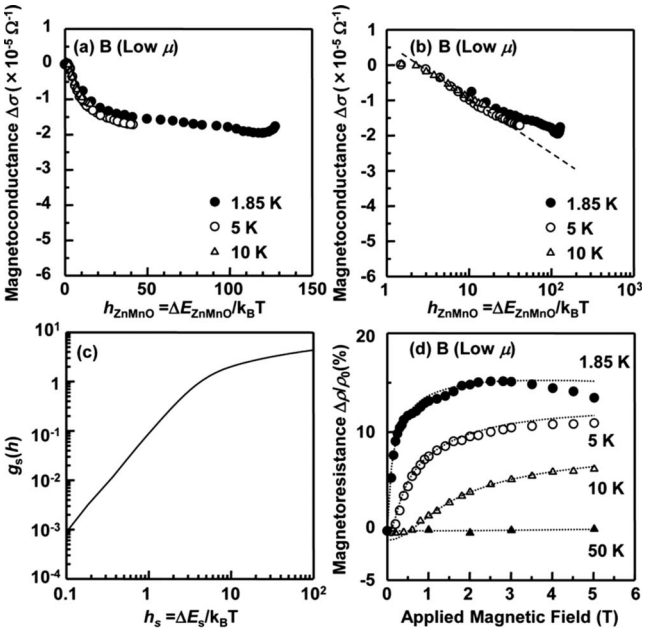

FIG. 7. [(a) and (b)] MC behavior $\Delta\sigma$ for sample B as a function of h_{ZnMnO}. Broken lines are a guide for the eyes. (c) Function $g_s(h)$ is obtained by numerically integrating Eq. (5). (d) Dotted lines are fitted to the experimentally obtained MR for sample B using Eq. (4). Closed circles, open circles, and closed triangles, respectively, represent MR measured at 1.85, 5, and 10 K.

$$\Delta E_{\mathrm{ZnMnO}}(H) \approx x_{\mathrm{eff}}\alpha N_0 S B_s(H). \tag{3}$$

The change in the $\Delta E_{\mathrm{ZnMnO}}$ against the applied magnetic field is expected to be proportional to the Brillouin function. Because the carriers are conducting in the ZnO channel layer, the spin-splitting energy of subband in the ZnO layer, indicated as ΔE_{ZnO}, are expected to be responsible for magnetoresistance $\Delta\rho/\rho_0$ and magnetoconductivity $\Delta\sigma$. Therefore, the correlation between $\Delta E_{\mathrm{ZnMnO}}$ and ΔE_{ZnO} must be discussed as follows. To evaluate this correlation, MR analyses were performed using the index of spin-splitting energy h_{ZnMnO}, which is $\Delta E_{\mathrm{ZnMnO}}/k_{\mathrm{B}}T$. Figure 7(a) presents the correlation between h_{ZnMnO} and $\Delta\sigma$ for sample B with low μ. For sample B, $\Delta\sigma$ decreases concomitantly with increasing h_{ZnMnO}. Changing the horizontal axis of Fig. 7(a) to the logarithm of h_{ZnMnO}, as shown in Fig. 7(b), the linear relation between $\Delta\sigma$ and the logarithm of h_{ZnMnO} is obtained irrespective of the temperature. Therefore, the relation between $\Delta\sigma$ and h_{ZnMnO} can be given as

$$\Delta\sigma(H) \propto \log(h_{\mathrm{ZnMnO}}). \tag{4}$$

Then, the experimentally obtained $\Delta\sigma$ is compared with the theoretical magnetoconductance (MC; $\Delta\sigma_s$) in a 2D system, which is expressed as Eq. (5) (Ref. 28)

$$\Delta\sigma_s(H) = -\frac{e^2}{\hbar}\frac{F_\sigma}{4\pi^2}g(h_s),$$

$$\text{with } h_s = \Delta E_s/k_{\mathrm{B}}T. \tag{5}$$

Here, F_σ is the screening parameter for the Coulomb interaction, ΔE_s is the spin-splitting energy, and $g(h_s)$ is the function dependent on h_s. Here, $g(h_s)$ is expressed as

$$g(h_s) = \int_0^\infty d\Omega \frac{d^2}{d\Omega^2}[\Omega N(\Omega)]\ln\left|1 - \frac{h_s^2}{\Omega^2}\right| \tag{6}$$

with

$$N(\Omega) = \frac{1}{\exp(h_s) - 1}. \tag{7}$$

The analytic expression for $g(h_s)$ is given in Ref. 29. Then, the function $g(h_s)$ can be numerically computed. As shown in Fig. 7(c), $g(h_s)$ changes against h_s. They have the limiting behaviors of $g(h_s)$

$$g(h) = 0.084h_s^2, \text{ for } h_s \ll 1 \tag{8}$$

and

$$g(h) = \ln(h_s/1.3), \text{ for } h_s \gg 1. \tag{9}$$

Using Eq. (9), when $h_s \gg 1$, $\Delta\sigma_s$ is expressed as

$$\Delta\sigma_s(H) = -\frac{e^2}{\hbar}\frac{F_\sigma}{4\pi^2}\ln(h_s/1.3). \tag{10}$$

The theoretical MR can be calculated using h_s and the following equation:

$$\mathrm{MR}(H) = \frac{\rho(H) - \rho(0)}{\rho(0)} = -\rho(H) \times \Delta\sigma_s(H). \tag{11}$$

In this case, $\Delta\sigma_s$ is proportional to the logarithm of h_s. When h_{ZnMnO} is used to calculate the theoretical MR instead of h_{ZnO}, $\Delta\sigma_s$ is expected to be the experimentally obtained relation shown as Eq. (4). The theoretical MR calculated using h_{ZnMnO} was compared with experimental MR. The theoretically calculated MR curves at elevated temperature are shown in Fig. 7(d) together with the experimentally obtained MR curves for sample B. As fitting parameters, F_σ of 0.7, 0.9, 0.9, and 0.9 were used, respectively, at 1.85, 5, 10, and 50 K. The experimental MR values can be well fitted to the theoretical ones, meaning that h_{ZnO} increases in proportional to h_{ZnMnO}. Therefore, it is suggested that ΔE_{ZnO} is proportional to $\Delta E_{\mathrm{ZnMnO}}$ under applied magnetic fields, and the correlation between ΔE_{ZnO} and $\Delta E_{\mathrm{ZnMnO}}$ is expressed as

$$\Delta E_{\mathrm{ZnO}} \propto \Delta E_{\mathrm{ZnMnO}}. \tag{12}$$

The experimental positive MR for sample B shows good agreement with the theoretical positive MR in 2D system, similarly to that for $Cd_{0.8}Mg_{0.2}Te/Cd_{1-x}Mn_xTe/Cd_{0.8}Mg_{0.2}Te$ modulation-doped quantum well.[27] For sample B, the Mn ions exist in ZnO channel because of large interface broadening, and the 2D conduction electrons directly interact with Mn *d* spins in ZnO channel.

Figure 8(a) shows $\Delta\sigma$ for sample A with high μ as a function of h_{ZnMnO}. The value of $\Delta\sigma$ linearly decreases concomitantly with increasing h_{ZnMnO}. Converting the horizontal axis from h_{ZnMnO} to $\Delta E_{\mathrm{ZnMnO}}$, Fig. 8(b) is obtained. All $\Delta\sigma$ measured at all temperatures overlap to a single straight line, suggesting that $\Delta\sigma$ for sample A is proportional to $\Delta E_{\mathrm{ZnMnO}}$ and h_{ZnMnO}, as described in Eq. (13)

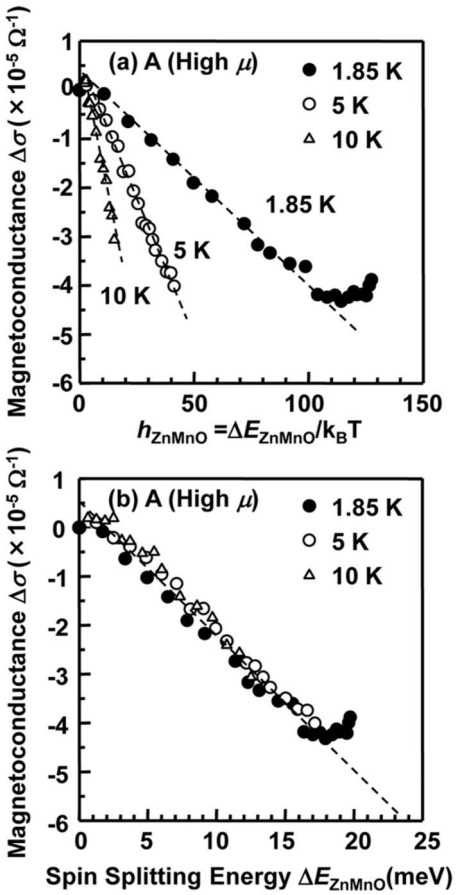

FIG. 8. (a) MC behavior $\Delta\sigma$ for sample A as a function of h_{ZnMnO}. (b) MC behavior $\Delta\sigma$ for sample A as a function of $\Delta E_{\mathrm{ZnMnO}}$. Closed circles, open circles, and open triangles, respectively, represent MC measured at 1.85, 5, and 10 K. Broken lines are a guide for the eyes.

$$\Delta\sigma \propto h_{\mathrm{ZnMnO}}, \Delta E_{\mathrm{ZnMnO}}. \tag{13}$$

In addition, using Eq. (3), this can be approximated as

$$\Delta\sigma \propto B_s(H), \tag{14}$$

Eq. (11) gives

$$\mathrm{MR}(H) \propto B_s(H). \tag{15}$$

To date, the positive MR obtained Mn-doped II-VI DMS bulk is explainable by quantum corrections to conductivity under the influence of the electron-electron interaction generated by spin-splitting energy in DMS. Sample B, with low μ, exhibits typical MR behavior of DMS in a low-dimensional system. However, no report describes observation of Brillouin-function-like positive MR behavior observed for sample A with high μ. Therefore, for sample A, the spin-dependent transport generated by the magnetic interaction at the ZnO channel/$Zn_{0.88}Mn_{0.12}O$ barrier interface might be observed by the suppression of interface broadening.

E. Origin of the Brillouin-function-like MR

Because the $Zn_{0.88}Mn_{0.12}O$/ZnO heterostructure with high μ has the interface with smaller interface broadening, ΔE_{ZnO} for sample A is assumed to be much smaller than that for sample B. When $h_{\mathrm{ZnO}} \ll 1$, Eqs. (8) and (15) give

$$\Delta E_{\mathrm{ZnO}} \propto \sqrt{\Delta E_{\mathrm{ZnMnO}}} \text{ as } h_{\mathrm{ZnO}} \ll 1. \tag{16}$$

Here, ΔE_{ZnO} is proportional to a square root of $\Delta E_{\mathrm{ZnMnO}}$, similarly to the correlation between the spin splitting in CdTe well and $Cd_{1-x}Mn_xTe$ barrier characterized using magneto-optical measurements for the $Cd_{1-x}Mn_xTe$/CdTe/$Cd_{1-x}Mn_xTe$ ($x \geq 0.20$) and $Cd_{0.89}Zn_{0.11}Te$/CdTe/$Cd_{1-x}Mn_xTe$ ($x \geq 0.20$) quantum wells with magnetic barrier.[30,31] Therefore, the origin of Brillouin-function-type MR is suggested as a wave function of the carriers in the ZnO channel layer penetrating into the $Zn_{0.88}Mn_{0.12}O$ barriers, and ΔE_{ZnO} is induced by the different penetration probability of the carriers with up-spin state and down-spin state because the $Zn_{0.88}Mn_{0.12}O$ barriers induce variation in the barrier height of the up-spin state and down-spin state. Further research has revealed that some heterostructures with μ close to the calculated μ_{total} show Brillouin-function-like MR, while other samples with much lower μ show 2D DMS MR behavior, supporting that the interface broadening is responsible for the spin-dependent transport of $Zn_{0.88}Mn_{0.12}O$/ZnO heterostructures.

For the $Zn_{0.88}Mn_{0.12}O$/ZnO heterostructure, results show that the different penetration probability of the wave function of the up-spin carriers and down-spin carriers into the $Zn_{0.88}Mn_{0.12}O$ barriers is responsible for spin-dependent transport. For the *n*-type heterointerface, however, ΔE_{ZnO} is small because $h_{\mathrm{ZnO}} \ll 1$ for sample A with high μ. Formation of two-dimensional hole gas at the heterointerface produces huge spin-splitting energy because the *p-d* exchange interaction $|N\beta|$ is 2.7 eV[32] and the ferromagnetic interaction is expected to be exhibited above room temperature.

IV. CONCLUSIONS

Using $Zn_{0.88}Mn_{0.12}O$/ZnO heterostructures, spin-dependent transport that occurred at the interface was investigated. The heterostructures showed two kinds of MR behavior. The heterostructure with low μ shows 2D DMS MR behavior, suggesting that *s-d* exchange interaction is directly generated between Mn *d* spins in ZnO channel and conduction electrons because of large interface broadening. On the other hand, MR behavior for the heterostructure with high μ was well fitted to the Brillouin function with $S=5/2$, suggesting that the effect of interface broadening on the MR is suppressed. Results show that the difference of the penetration probability of the wave function of up-spin carriers and down-spin carriers in ZnO subband into the $Zn_{0.88}Mn_{0.12}O$ barrier layer is responsible for Brillouin-function-like MR.

ACKNOWLEDGMENTS

This research was partially supported by a Ministry of Education, Culture, Sports, Science and Technology (MEXT) Grant-in-Aid for Scientific Research on priority areas under Grant No. #19033005 and JSPS Fellows under Grant No. #20-5643.

[1] H. Ohno, D. Chiba, F. Matsukura, T. Omiya, E. Abe, T. Dietl, Y. Ohno, and K. Ohtani, Nature (London) **408**, 944 (2000).
[2] R. Fielderling, M. Keim, G. Reuscher, W. Ossau, G. Schmidt, A. Waag, and L. W. Molenkamp, Nature (London) **402**, 787 (1999).
[3] M. Tanaka and Y. Higo, Phys. Rev. Lett. **87**, 026602 (2001).
[4] A. M. Nazmul, S. Sugahara, and M. Tanaka, Phys. Rev. B **67**, 241308(R) (2003).
[5] S. Ghosh, V. Sih, W. H. Lau, D. D. Awschalom, S.-Y. Bae, S. Wang, S. Vaidya, and G. Chapline, Appl. Phys. Lett. **86**, 232507 (2005).
[6] T. Dietl, H. Ohno, F. Matsukura, J. Cibert, and D. Ferrand, Science **287**, 1019 (2000).
[7] T. Edahiro, N. Fujimura, and T. Ito, J. Appl. Phys. **93**, 7673 (2003).
[8] K. Masuko, A. Ashida, T. Yoshimura, and N. Fujimura, J. Appl. Phys. **103**, 07D124 (2008).
[9] K. Masuko, H. Sakiyama, A. Ashida, T. Yoshimura, and N. Fujimura, Phys. Status Solidi C **5**, 3107 (2008).
[10] K. Masuko, A. Ashida, T. Yoshimura, and N. Fujimura, J. Vac. Sci. Technol. A **27**, 1760 (2009).
[11] K. Masuko, A. Ashida, T. Yoshimura, and N. Fujimura, J. Appl. Phys. **103**, 043714 (2008).
[12] M. Nakayama, H. Tanaka, K. Masuko, T. Fukushima, A. Ashida, T. Yoshimura, and N. Fujimura, Appl. Phys. Lett. **88**, 241908 (2006).
[13] J. K. Furdyna, J. Appl. Phys. **64**, R29 (1988).
[14] Y. Oda, K. Masuko, M. Tabuchi, N. Fujimura, and Y. Takeda, Extended Abstracts of the 54th Autumn Meeting of the Japan Society of Applied Physics, Aoyama Gakuin University, 2007, No. 2, p. 1027.
[15] T. Oshio, K. Masuko, A. Ashida, T. Yoshimura, and N. Fujimura, J. Appl. Phys. **103**, 093717 (2008).
[16] T. Ando, J. Phys. Soc. Jpn. **51**, 3900 (1982).
[17] S. Hiyamizu, J. Saito, K. Nanbu, and T. Ishikawa, Jpn. J. Appl. Phys. **22**, L609 (1983).
[18] W. Walukiewicz, H. E. Ruda, J. Lagowski, and H. C. Gatos, Phys. Rev. B **30**, 4571 (1984).
[19] J. H. Davis, *The Physics of Low-dimensional Semiconductors* (Cambridge University Press, Cambridge, 2004), p. 385.
[20] T. Andrearczyk, J. Jaroszyński, G. Grabecki, T. Dietl, T. Fukumura, and M. Kawasaki, Phys. Rev. B **72**, 121309(R) (2005).
[21] D. A. Muller, L. Fitting Kourkoutis, M. Murfitt, J. H. Song, H. Y. Hwang, J. Silcox, N. Delby, and O. L. Krivanek, Science **319**, 1073 (2008).
[22] Wanli Li, G. A. Csáthy, D. C. Tsui, L. N. Pfeiffer, and K. W. West, Appl. Phys. Lett. **83**, 2832 (2003).
[23] Y. Fua and M. Willander, J. Appl. Phys. **88**, 288 (2000).
[24] For a review, see T. Dietl, J. Phys. Soc. Jpn. **77**, 031005 (2008).
[25] M. Sawicki, T. Dietl, J. Kossut, J. Igalson, T. Wojtowicz, and W. Plesiewicz, Phys. Rev. Lett. **56**, 508 (1986)
[26] Q. Xu, L. Hartmann, H. Schmidt, H. Hochmuth, M. Lorenz, D. Spemann, and M. Grundmann, Phys. Rev. B **76**, 134417 (2007).
[27] J. Jaroszyński, T. Andrearczyk, G. Karczewski, J. Wróbel, T. Wojtowicz, D. Popović, and T. Dietl, Phys. Rev. B **76**, 045322 (2007).
[28] P. A. Lee and T. V. Ramakrishnan, Rev. Mod. Phys. **57**, 287 (1985).
[29] M. S. Burdis and C. C. Dean, Phys. Rev. B **38**, 3269 (1988).
[30] Using the experimental results for samples M97 QW2, M336, M340, M162, M177, and M 178 in J. A. Gaj, W. Grieshaber, C. Bodin-Deshayes, J. Cibert, G. Feuillet, Y. Merle d'Aubigne, and A. Wasiela, Phys. Rev. B **50**, 5512 (1994), we replotted squared ΔE_{CdTe} as function of $\Delta E_{\mathrm{CdMnTe}}$. The results suggested that the relation between ΔE_{CdTe} and $\Delta E_{\mathrm{CdMnTe}}$ is a square-root like relation.
[31] W. Grieshaber, A. Haury, J. Cibert, Y. M. d'Aubigne, A. Wasiela, and J. A. Gaj, Phys. Rev. B **53**, 4891 (1996).
[32] T. Mizokawa, T. Nambu, A. Fujimori, T. Fukumura, and M. Kawasaki, Phys. Rev. B **65**, 085209 (2002).